Microparticle collection and concentration *via* a miniature surface acoustic wave device

Ming K. Tan, James R. Friend* and Leslie Y. Yeo

Received 11th December 2006, Accepted 20th March 2007
First published as an Advance Article on the web 18th April 2007
DOI: 10.1039/b618044b

The ability to detect microbes, pollens and other microparticles is a critically important ability given the increasing risk of bioterrorism and emergence of antibiotic-resistant bacteria. The efficient collection of microparticles *via* a liquid water droplet moved by a surface acoustic wave (SAW) device is demonstrated in this study. A fluidic track patterned on the SAW device directs the water droplet's motion, and fluid streaming induced inside the droplet as it moves along is a key advantage over other particle collection approaches, because it enhances microparticle collection and concentration. Test particles consisted of 2, 10, 12 and 45 μm diameter monodisperse polystyrene and melamine microparticles; pollen from the *Populus deltoides*, *Kochia scoparia*, *Secale cerale*, and *Broussonetia papyrifera* (Paper Mulberry) species; and *Escherichia coli* bacteria. The collection efficiency for the synthetic particles ranged from 16 to 55%, depending on the particle size and surface tension of the collection fluid. The method was more effective in collecting pollen and the bacteria with an efficiency of 45–68% and 61.0–69.8%, respectively. Pollen collection was strongly influenced by its diameter, size, and surface geometry in a manner contrary to initial expectations. Reasons for the consistent yet unexpected collection results include leaky SAW pressure boundary segregation and shear-induced concentration of larger particles, and the subtle effects of wetting interactions. These results demonstrate a new method for collecting microparticles requiring only about one second per run, and illustrate the inadequacy of using synthetic microparticles as a substitute for their biological counterparts in experiments studying particle collection and behavior.

Introduction

Threats to society from terrorist acts and the emergence of antibiotic-resistant bacteria has encouraged research on early warning detection systems to quickly and effectively monitor pathogen outbreaks.[1,2] Environmental air monitoring through rapid detection of other airborne particles, including seasonal pollen, fungi, and bacteria would also be beneficial. A small and portable biosensor to detect the presence of these particles would facilitate work on the prevention and mitigation of outbreaks. In principle, an effective airborne microparticle sampling device should be able to collect and concentrate airborne microparticles into a carrier for subsequent detection downstream through a biosensor component. Here, we will focus our effort on determining the mechanism underlying the surface acoustic wave (SAW)-driven collection of synthetic particles, pollen, and *Escherichia coli* bacteria in which a liquid medium is used as the carrier to represent the target applications; the particle-laden carrier can then be ported to a biodetection or biosensing component in the same integrated microfluidic biosensor device.

Airborne microparticle collection using electrowetting has been demonstrated by Zhao and Cho.[1] In this paper, we introduce a new methodology for airborne microparticle collection using a SAW device. SAW devices have been used for decades for telecommunication signal processing and filtering;[3] their sensitivity to very small changes in mass on the surface due to resonant frequency shifts has also enabled the use of SAW devices as microsensors.[4] SAW devices may also be used for fluid manipulation in addition to characterization, including droplet transport[5–8] and atomization.[9–12] As will be shown, an advantage of SAW devices for microparticle collection over the electrowetting approach is the generation of an acoustic-streaming flow recirculation inside the droplet, illustrated by Fig. 1. This appears to assist the collection and retention of microparticles and the subsequent concentration of the collected microparticles within the droplet.

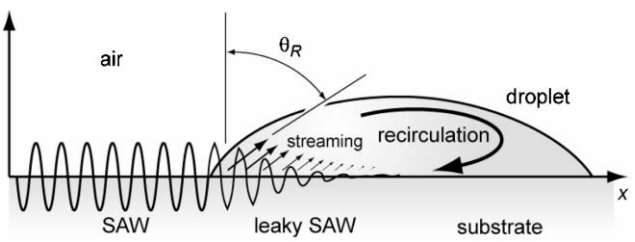

Fig. 1 Schematic illustration of the Rayleigh SAW propagating on the surface of a piezoelectric substrate and its interaction with a liquid droplet. Acoustic streaming is induced by the SAW due to leakage of the acoustic energy into the liquid at the Rayleigh angle θ_R.

Micro/Nanophysics Research Laboratory, Monash University, Clayton, Victoria 3800, Australia. E-mail: james.friend@eng.monash.edu.au; Tel: +61 3990 51089

In addition, research has shown that micro- and nanoparticles pose considerable risk to human health.[13] It is therefore desirable that practical particle sampling devices should also be able to collect and concentrate nanoparticles, depending on the application. To do so effectively, the size of the carrier, *i.e.* the liquid droplet in this case, should be reduced accordingly. This scalability is possible in the proposed device by increasing the SAW excitation frequency, thus facilitating the actuation or manipulation of smaller carrier droplets.

Droplet manipulation using SAW

Direct generation of surface acoustic waves on a piezoelectric substrate using interdigital electrodes was first reported by White and Voltmer.[14] The devices are fabricated using photolithography to pattern a metallic coating, typically Al, into the interdigital pattern. As shown in Fig. 1, the SAW is generated along the surface of the piezoelectric substrate by applying a high-frequency electromagnetic signal to the interdigital transducer (IDT). Depending on the orientation of the piezoelectric crystal cut, many different vibration modes can be excited in the substrate.[4]

If the substrate consists of 127.68 rotated *Y–X* cut, *X*-propagating $LiNbO_3$, Rayleigh waves can be generated in which two mechanical acoustic wave components are generated, namely, a compressional component along the direction of propagation and a transverse component perpendicular to the surface. Upon excitation, the displacement of the substrate normal to the substrate surface is larger than the displacement along the direction of SAW propagation since the elastic solid is more free to vibrate transverse to the surface.[3] Manipulation of a liquid droplet on SAW substrates depends strongly on the diffraction of the compressional wave into the droplet.[5–8] Within the substrate, the compressional and transverse wave displacements decay exponentially with increasing distance from the substrate surface until, at 4–8 acoustic wavelengths below the free surface, the displacements are negligible.[3]

Upon placing a water droplet upon the surface of the substrate to interact with the SAW, the in-plane, axially-polarized compressional displacement component is diffracted at the *Rayleigh angle* into the droplet, generating so-called *Leaky SAW* (LSAW)[15,16] due to the 'leakage' of the radiation into the liquid. The Rayleigh angle is defined as $\theta = \sin^{-1}(c_w/c_s)$, where c_w is the Rayleigh wave velocity in the liquid and c_s is that in the solid. The leaky component of the SAW induces an acoustic pressure gradient inside the droplet, giving rise to *acoustic streaming*. This streaming force is the result of acoustic energy flux dissipation within the fluid; it is balanced with forces due to fluid viscosity and inertia. For high-power ultrasonic excitation, the induced streaming motion imparts momentum to the fluid, giving acoustic-streaming jets[17] or even atomization.[9–12] At lower excitation power, the induced streaming motion inside the droplet causes internal recirculation, bounded by capillary forces acting along the free surface of the droplet. At higher excitation powers, but below that which causes jetting or atomization, the entire droplet translates along the direction of the SAW propagation due to a net force arising from the leaky component of the SAW.

Experimental

Standard photolithography was used to fabricate a collection of 15 mm-wide, 45 mm-long, and 0.6 mm-thick SAW devices using 127.68°-rotated *Y–X* cut single-crystal $LiNbO_3$. A pair of bidirectional IDTs with a relatively low resonance frequency of 8.6 MHz was fabricated on the SAW substrate. A sinusoidal electrical signal was applied to the input IDT at a frequency matching the IDT resonance and at a power sufficient to move fluid droplets as described later, while the output IDT was left in an open-circuit condition. In order to minimize wave reflection, a viscous and dense adhesive gel (α-gel®, Geltec Ltd., Yokohama, Japan) was attached to the surface above the output IDT. Any wave energy reflected from the opposite end would interfere with the propagating wave and cause the droplet to slow down or stop. Since $LiNbO_3$ is hydrophilic, a high driving force is typically required to move a water droplet along the surface.[8] To mitigate this problem and further enhance the droplet motion, a narrow strip of 10 μm-thick Teflon® (polytetrafluoroethylene) tape, 3.5 mm wide × 17 mm long, was used as a hydrophobic fluidic track along the SAW propagation axis to guide the drop's motion and to reduce the adhesion forces along the liquid–solid interface.[5–8]

An intermittent sinusoidal signal was used to drive the SAW device through a pair of pogo-stick contact probes. Two different gated waveforms were used, 100 kλ† wavelengths on/100 kλ off, and 100 kλ on/50 kλ off. The excitation time for a single 100 kλ on/100 kλ off cycle is approximately 10 ms, based on the 8.6 MHz resonance frequency. By reducing the time the signal is off, the average signal magnitude is larger, providing more acoustic energy into the droplet.

For each experimental run, a 10 μl deionized (DI) water droplet was dispensed onto the fluidic track using a micropipette on the end closest to the input IDT. The droplet spans the width of the fluidic track. Before testing for particle collection, the appropriate input voltage signal level required to smoothly move the droplet from the input IDT to the output IDT, without splitting, jetting or atomization, was determined by slowly increasing the applied voltage from zero and repeating the run until consistent and repeatable motion was obtained. The droplet was collected using a micropipette and the surface cleaned using lint-free cleanroom wipes, DI water, and pressurized clean dry air. A thin layer of the sample particles was spray-deposited across the SAW device, a 10 μl droplet was placed near the input IDT, and the quality of the particle collection was then assessed as described later. This process was repeated 15 times for each particle size and type.

A CCD microscope (SCALAR M2, Scalar Ltd., Tokyo, Japan) was used for image capture before and after the water droplet was swept along the hydrophobic track. To prepare the images for subsequent processing, the color information in each image was discarded, and the brightness range of the image was normalized to 256 grayscale levels using Photoshop CS (Adobe Systems Inc.). All images were processed in the same way to ensure consistency; the images were subsequently subjected to a pixel intensity analysis using MATLAB (The MathWorks Inc.). The standard deviation in intensity for a

† One wavelength is 1λ.

particular image was calculated using all values in the intensity matrix for the image. The particle collection efficiency can then be evaluated; by definition,[18,19]

$$\text{Particle collection efficiency} = \frac{(\text{light intensity after collection} - \text{light intensity before collection})}{\text{light intensity before collection}} \times 100\%$$

The motion of the swirling particles inside the droplet due to acoustic streaming was captured using a high-speed video camera (Olympus iSpeed, Olympus, Tokyo, Japan) set at 60 frames per second and mounted to a long-distance microscope (InfiniVar, Boulder, Colorado). The droplets were also viewed from the side to gain more information on the particle collection mechanism, especially important for some cases where the particles appeared to be suspended in a thin wetting precursor film above the substrate or were simply left behind while the droplet passed by along the track.

To better understand the factors which contribute to the collection efficiency, we have used synthetic and pollen particles and *Escherichia coli* bacteria (Sigma-Aldrich, Castle Hill NSW). The synthetic particles consisted of monodisperse polystyrene and melamine spherical microbeads (Sigma-Aldrich Australia, Castle Hill NSW and BioScientific, Gymea NSW, respectively); polystyrene is hydrophobic, while melamine is hydrophilic. Four particle diameters were used: 2, 10, 12, and 45 μm; each were made from either polystyrene or melamine. Using such a variety of particles, the dependence of wettability and diameter on the collection efficiency can be elucidated. The pollens and bacteria, on the other hand, provide a more realistic assessment of SAW device use in biological particle collection. Four different types of pollen were employed, from the eastern cottonwood tree *Populus deltoides*, the fireweed plant *Kochia scoparia*, the common rye grass *Secale cerale*, and the Tapacloth tree *Broussonetia papyrifera* (Paper Mulberry) (Sigma-Aldrich, Castle Hill NSW, BioScientific, Gymea NSW Australia). These pollens were selected due to their availability in Australia despite tight environmental regulations, and represent three different groups prevalent in Australian air samples from trees, weeds, and grass. For the purposes of collection in a fluid, pollens may be categorised by their exine surface profile and overall size as summarized in Table 1. *Populus deltoides*, *Broussonetia papyrifera* and *Secale cerale* have a scabrate surface whilst *Kochia scoparia* has a perforate surface.[18,19] Scanning electron microscope (SEM) micrographs are provided in Fig. 2 for the pollen used in this study; note the difference between the pollens' porous and hollow morphology and the monodisperse synthetic particles' homogeneous and smooth microspherical shape. It is important to note here that a large majority of pollens, including all the ones used in this study, are hydrophilic.[20] *E. coli* bacteria, gram-negative elongated rod-shaped bacteria, 1–2 μm long and 100–200 nm in diameter, is a lab-safe example of potentially airborne[21] bacteria that would be important to detect; Neill *et al.*[22] provide detailed information on *E. coli* omitted here for brevity.

Table 1 Pollen characteristics

	Broussonetia papyrifera	*Populus deltoides*	*Secale cerale*	*Kochia scoparia*
Size/μm	12–13	25–35	49–58	20–35
Surface profile	Scabrate	Scabrate	Scabrate	Perforate

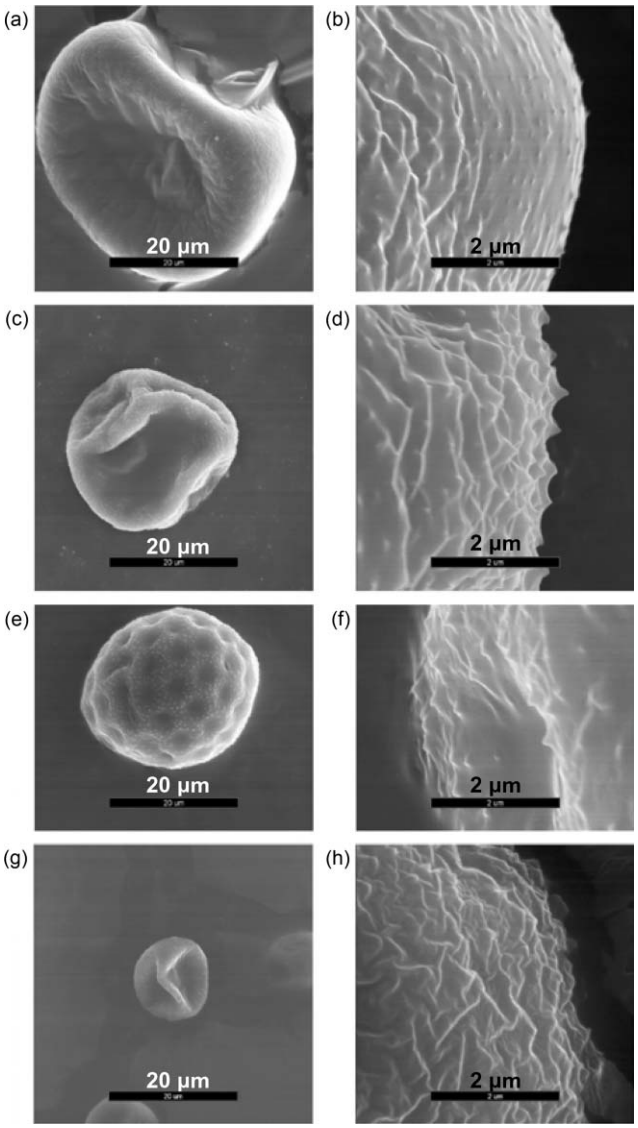

Fig. 2 SEM micrographs illustrating the pollen morphology when dry. The left panels (a), (c), (e), and (g) show a typical single pollen particle at 2000× magnification while the right panels (b), (d), (f), and (h) show a 20 000× magnified view of the pollen surface. (a, b) Grass pollen (*Serale cerale*), (c, d) tree pollen (*Populus deltoides*), (e, f) weed pollen (*Kochia scoparia*), and (g, h) tree pollen (*Broussonetia papyrifera*) are a representative sampling of typical pollens.

Results and discussion

The collection efficiency for the synthetic and pollen microparticles are tabulated in Table 2 and depicted in Fig. 3. Tables 3 and 4 provide an assessment of the significance of changing the particle size on the collection efficiency through the use of Student's two-tailed *t*-test.[23] The hypothesis statements were, H_A: groups have unequal collection efficiency, and H_0: groups have equal collection efficiency; statistical

Table 2 Collection efficiency for synthetic particles and pollen

Particle type	Collection efficiency (%) Mean	(95% Confidence interval for mean)
Melamine 2 μm	22.4	16.5–28.0
Melamine 10 μm	23.3	18.0–27.9
Melamine 12 μm	25.3	18.2–32.3
Melamine 45 μm	34.9	26.7–43.1
Polystyrene 2 μm	46.1	36.9–55.2
Polystyrene 10 μm	34.6	25.7–46.1
Polystyrene 12 μm	31.4	20.1–42.7
Polystyrene 45 μm	29.1	17.8–40.4
Secale cerale pollen	65.6	63.4–67.8
Kochia scoparia pollen	49.4	45.8–53.1
Populus deltoides pollen	62.4	58.4–66.5
Broussonetia papyrifera pollen	61.3	56.5–66.0

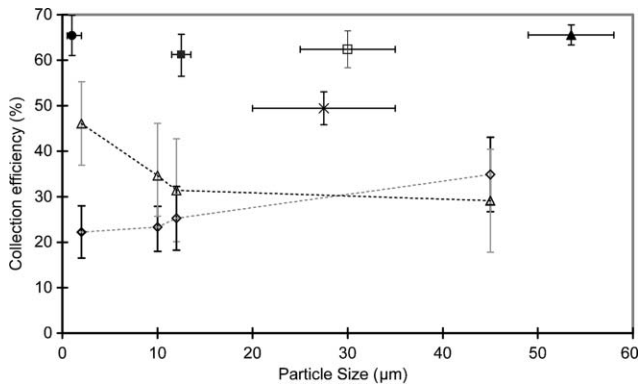

Fig. 3 Collection efficiency for different microparticles; the center point is the mean for 15 tests and the error bar indicates the mean's 95% confidence interval. The collection efficiency decreases as the particle size increases for hydrophobic particles and increases as the particle size increases for hydrophilic particles. (◇ – Melamine, Δ – polystyrene, × – *Kochia scoparia*, □ – *Populus deltoides*, ■ – *Broussonetia papyrifera*, ▲ – *Secale cerale*, and ● – *Escherichia coli* bacteria.)

significance was treated as equivalent to having a probability of less than 0.05 that the reported result would occur by chance. Each data set has a normal distribution and passes a test of independence from other data sets which together verify the validity of using the *t*-test. The sample size for each group of data was 15 runs. The results indicate that the collection efficiencies for the synthetic microparticles were generally lower than for the pollen. Comparing the 2, 10, 12 and 45 μm diameter synthetic particle results, the collection efficiency was

Table 3 Probability values from Student's two-tailed *t*-test to assess the significance of polystyrene microparticle diameter on the collection efficiency. There were statistically significant (probability $p < 0.05$) changes in the collection efficiency between the collection of particles 2 and 12 μm in diameter, and 2 and 45 μm in diameter

Size/μm	2	10	12	45
2		0.128	0.004	0.019
10			0.536	0.350
12				0.756
45				

Table 4 Probability values from Student's two-tailed *t*-test to assess the significance of melamine microparticle diameter on the collection efficiency. There were statistically significant changes in the collection efficiency between the collection of particles 2 and 45 μm in diameter, and 10 and 45 μm in diameter

Size/μm	2	10	12	45
2		0.085	0.484	0.012
10			0.573	0.014
12				0.068
45				

higher for smaller polystyrene (hydrophobic) particles while lower for smaller melamine (hydrophilic) particles. This is a surprising result, as one would intuitively expect that it would be more difficult to collect hydrophobic particles. As the particle size decreases, an increase in surface area-to-volume ratio would presumably increase the interfacial area and hence the interfacial energy required to wet the particle. The behavior for hydrophilic particles would be the opposite.

The reasons for the counter-intuitive result in Table 2 and Fig. 3 are subtle, assisted by viewing the droplet from the side as it collects the particles, shown in Fig. 4, in addition to the behavior from the top, shown in Fig. 5. The bulk liquid recirculation within the droplet arising due to acoustic streaming causes the 2 μm melamine particles to thoroughly disperse due to their higher surface area-to-volume ratio. Particles that end up near the side or trailing edges of the droplet are easily left behind as the droplet passes, since these areas have relatively low fluid velocities and exhibit unsteady flow behavior due to pinning and rapid release of the contact line around the periphery of the advancing droplet. However, the 10 and 45 μm melamine particles tended to collect near the interior of the droplet and so were less likely to be left behind, as shown by the clean state of the track after the droplet has passed [see Fig. 5(a)]. Thus, we observe better collection efficiencies with the larger melamine particles.

The SAW-induced pressure distribution within the droplet prevents the migration of larger particles toward the trailing end of the droplet. As the oscillatory pressure wave propagates from the substrate–droplet interface at the Rayleigh angle into the droplet, at the droplet's left in Fig. 4, a region of high pressure is formed along the propagation axis of the *leaky SAW*. Toward the left or trailing side of this boundary, the leaky SAW generates a higher-pressure region, and to the right or leading side of this quite distinct boundary, the pressure is near ambient.[24,25] By equating the drag force of the fluid on a particle with the force due to the pressure change, the effect of particle size on its ability to cross the boundary may be estimated – the equality implies the equilibrium of the forces on a particle being pushed across the boundary by the flow yet restrained by the unfavorable pressure change. Stokes' drag force is proportional to $d\eta u$; the three terms are particle diameter, fluid dynamic viscosity, and the relative velocity between the particle and surrounding fluid, respectively. The force due to the pressure change is proportional to $\Delta p d^2$. Equating the two, it can be seen that as the particle diameter increases the pressure change Δp becomes more significant and will prevent the passage of particles beyond a certain critical size. To estimate the scale of this critical size, the force equality

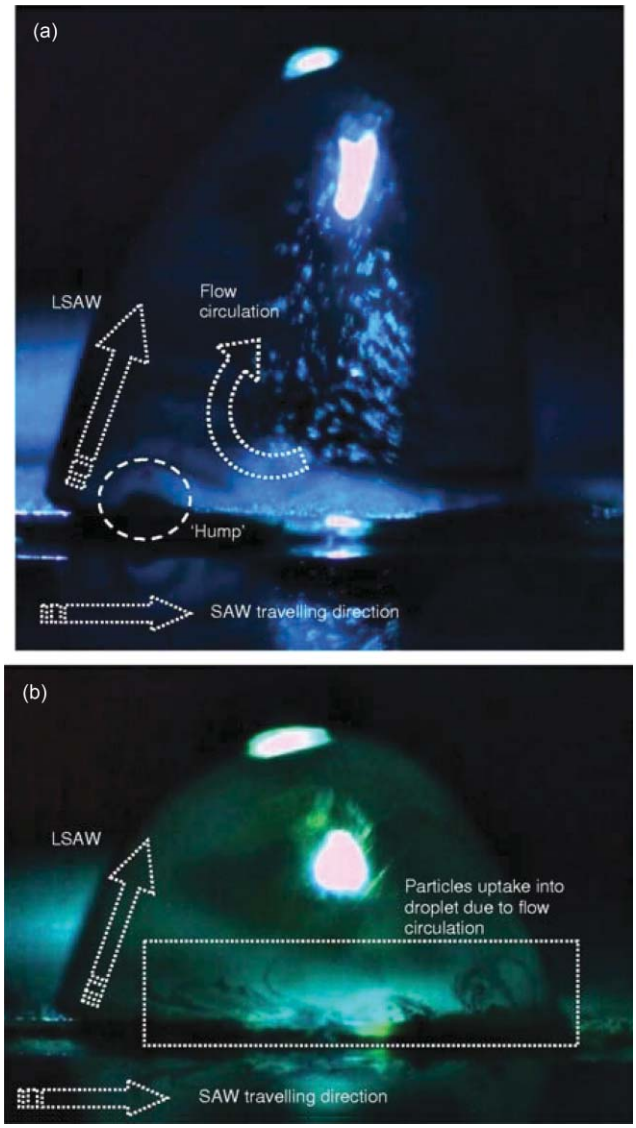

Fig. 4 Image showing the collection mechanism of synthetic microparticles inside the water droplet for (a) 12 μm diameter polystyrene, and (b) 2 μm diameter polystyrene. The high pressure narrow beam streaming jet deformed the droplet shape and caused the recirculation flow. The 'Hump' was formed at the junction where the streaming jet and recirculated flow meet – the stagnation point. Particle uptake into the droplet was observed to result from recirculation flow and enhanced by the streaming jet at the trailing edges.

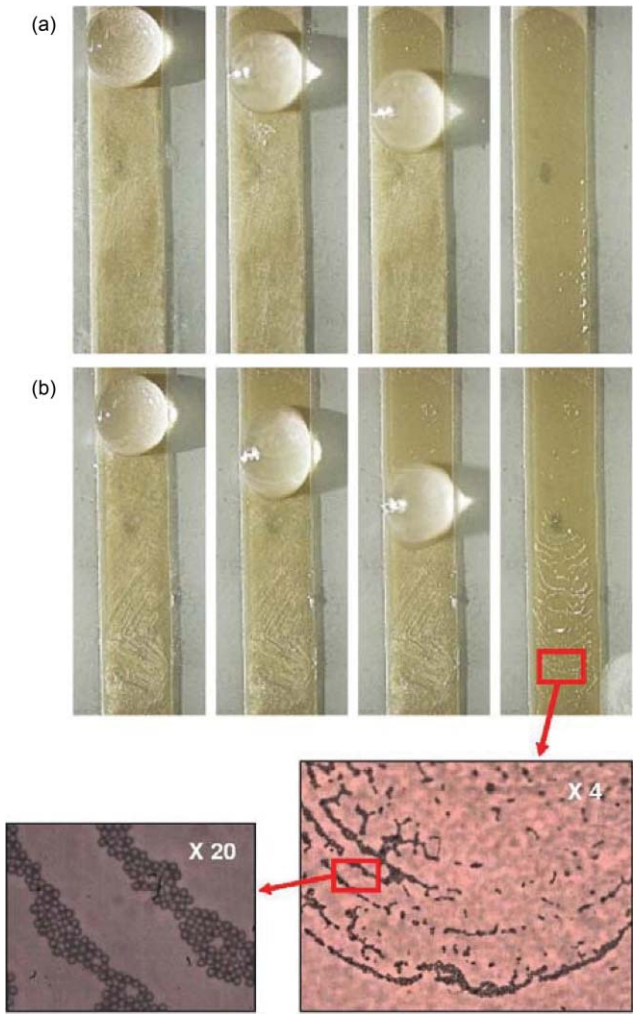

Fig. 5 Sequential images showing particles sampled on the fluidic track for 10 μm (a) melamine and (b) polystyrene particles. The droplet is moving top to bottom; the input and output IDTs are at the top and bottom, respectively, just outside the view in the photos. Melamine particles were left behind along the edges of the track as the droplet moved, especially near the bottom where the droplet was moving at its highest speed. Polystyrene particles were instead left behind in ring-like structures across the track. Further magnification of the rings shows that particles assembled in regimented monolayer rings rather than as random clusters.

gives $d \approx \eta u/\Delta p$; each of the terms at the right may be estimated to be 10^{-3} Pa s, 10^{-2} m s^{-1}, and 10^{1} Pa (across the width of a particle), respectively,[25] giving $d \approx 1$ μm. Particles smaller than this approximate value can cross over from the leading to the trailing side of the droplet, while larger particles may not. Evidence of this phenomenon appears in the appearance of a 'hump' of particles pushed to the right of the pressure boundary in Fig. 4(a) for 12 μm particles, while 2 μm particles pass freely throughout the droplet in Fig. 4(b).

Curiously, the acoustic force on the particles themselves appears to be far lower than the Stokes' drag or the force due to the leaky SAW high-pressure boundary. The acoustic force is proportional to $kVEG$, a product of the wavenumber of the acoustic radiation, volume of the particle, acoustic energy, and the acoustic contrast factor, respectively.[26] For polystyrene, G is 1.05, and for the system in this study, $k \approx 10^{5}$ m^{-1}, $V \approx 10^{-18}$ m^{3} (for a 10 μm particle), and $E \approx 10^{0}$ W, giving an acoustic force of an order 10^{-13} N, two orders of magnitude smaller than the forces due to Stokes' drag or leaky SAW-induced pressure for a 10 μm polystyrene particle. Therefore, the induced motion of the particles appears to be an indirect phenomenon of the leaky SAW inducing fluid motion and a pressure boundary which together control the motion of the entrained particles picked up from the substrate.

It is likely that shear-induced migration also plays a role in causing large particles to collect in the interior of the droplet. This has been studied in further detail and reported in a separate paper in which this is exploited for bioparticle

trapping.[22] The shear-induced migration velocity scales as the square of the particle size, thus enabling the larger 10 μm particles to effectively cross the bulk acoustic-streaming convection streamlines from the high-shear regions in the outer periphery of the drop, where the velocity is higher, to populate the interior of the drop where the velocity and hence shear is lower.[27,28] The smaller 2 μm particles are, however, less likely to undergo shear-induced migration because the diffusion time scale is comparable to or greater than the acoustic-streaming convective time scale.[25] As such, the smaller particles tend to be suspended throughout the droplet, thus increasing their chance of entering the drop stagnation regions close to the side and trailing edges of the drop.

The 2 μm polystyrene particles were observed to constantly recirculate within the droplet in the direction of the streaming current, while the larger 10 and 45 μm polystyrene particles tended to accumulate at the bottom of the droplet and adjacent to the strongly hydrophobic Teflon® track. The internal recirculation managed to suspend the smaller particles and retain them, while the larger particles remained behind, giving a much lower collection efficiency. Further, it was found that the accumulation of the 10 and 45 μm polystyrene particles on the hydrophobic track surface diminished the leakage of SAW radiation into the drop, requiring a higher applied voltage to move the droplet.

As 10 μm polystyrene particles are collected along the track shown in Fig. 5(b), they are observed to form regimented rings behind the droplet, particularly near the bottom end of the track. A closer examination of the ring formation in Fig. 5(b) shows that the particles assemble into monolayer rings, *ca.* 20–160 μm wide with about a 200 μm gap between each ring. The monolayer ring formation can be attributed to the tendency of the hydrophobic polystyrene particles to minimize their contact with the water droplet. As such, the particles tend to aggregate at the three-phase (air–water–substrate interface) contact line of the droplet where a minimum of the particles' surface area is exposed to water. As the drop moves forward, this contact line is placed under increasing traction to be suddenly pulled forward several hundred microns, leaving a ring of particles behind on the substrate surface. The new contact line is subsequently filled with fresh particles repelled from the bulk that exploit this opportunity to minimize their contact with water. This process repeats itself along the track, thus explaning the observation of ring sequences. Resuspension of the particles back into the bulk, thus destroying the ring formation, is not observed because of insufficient acoustic-streaming convection to overcome the strong hydrophobicity of the particles. The above also explains why the larger 10 μm polystyrene particles are repelled from the bulk and accumulate at the substrate where it can minimize its contact with water, while the smaller 2 μm polystyrene particles are collected with far greater efficiency. The repulsion of the 10 μm particles from the bulk also suggests why shear-induced migration does not occur in the polystyrene particles as in the case of the melamine particles.

No such ring formation is observed in the sequence of collection images for the 10 μm melamine particles in Fig. 5(a). Instead, the figure shows that most deposited melamine particles are removed from the first half of the track, yet near the bottom, particles have been left behind along the edges of the track. This appears to be due to the saturation of the collection droplet, and the tendency of the particles to be swept laterally towards the side edges of the droplet.

The collection efficiency for pollen, on the other hand, appears to be dominated by the surface geometry and size of the pollen. The pollen was observed to accumulate at the front of the droplet. Owing to the direction of the internal streaming current and the presence of the high-pressure region generated by the leaky SAW radiation region described earlier, the pollen is prevented from moving to the trailing side of the droplet. The collection mechanism is similar to the generic model described above. As expected from the result for the synthetic particles, noting that the chosen pollens – like most pollens – are hydrophilic,[20] the collection efficiency increases as the pollen diameter increases. *Secale cerale*, with an approximate diameter of 49–58 μm, was collected with an efficiency of 63.4–67.8%, compared with the 58.4–66.5% collection efficiency of *Populus deltoides*, with an approximate diameter of 25–35 μm. *Broussonetia papyrifera*, the smallest of the pollens with an approximate diameter of 12–13 μm, was collected with an efficiency of 56.5–66.0%.

The exception is the *Kochia scoparia* weed pollen with a lower collection efficiency of 45.8–53.1%. This is attributed to the morphology and wetting characteristics of the pollen surface. Referring to Table 1, *Secale cerale*, *Populus deltoides* and *Broussonetia papyrifera* have the same scabrate surface topology as shown in Fig. 3. The perforate *Kochia scoparia* weed pollen and scabrate *Populus deltoides* tree pollen are approximately the same size but the former has a porous structure in addition to the spiked exine. The irregular surface of the scabrate *Populus deltoides* tree pollen therefore appears to aid its collection.

In any case, the collection efficiency of the pollens is always significantly higher (approximately 30%) than for comparably-sized hydrophilic melamine microparticles, as shown in Fig. 3. The enhancement in the collection efficiency is due to the rough surface morphology of the pollen compared with the smooth surface morphology of the synthetic particles. It is well known that as the surface roughness increases, a hydrophobic interface would appear *more* hydrophobic and a hydrophilic surface would appear *more* hydrophilic, as stipulated by Wenzel's law.[29,30] As a consequence, the wettability of the hydrophilic pollen is dramatically increased by the roughness, thereby enhancing its collection efficiency compared to hydrophilic synthetic particles of similar size.

To investigate the effect on the collection efficiency from changing the amount of particulate material deposited on the substrate, the amount of *Secale cerale* grass pollen was changed from 2.13 to 5.68 mg in 45 separate runs, representing a very light dusting to a dense covering of pollen. Table 5 shows that a significant change in the collection efficiency could not be detected over this range.

Representing bioparticles that a sensor might be designed to collect, *E. coli* was chosen for collection. Given the dangerous nature of anthrax and other bioparticles that might be used for terrorism, and the cautious nature of regulating agencies, we are limited in our choices of biological entities for collection. The collection efficiency ranged from 61.0 to 69.8% based on

Table 5 Probability values from Student's two-tailed *t*-test to assess the significance of grass pollen weight on collection efficiency; the probability results indicate no significant change in the collection efficiency due to the changes

Weight/mg	2.13–2.45	3.11–3.61	4.56–5.68
2.13–2.45		0.628	0.244
3.11–3.61			0.380
4.56–5.68			

22 runs, slightly better than the pollen collection efficiency. Given that *E. coli*, like many bacteria, is hydrophobic,[31] and the collection efficiency improves in our device as the hydrophobic particle size is *reduced*, this collection result is consistent with the counter-intuitive results achieved in collecting polystyrene particles as described earlier. Further, *E. coli* with its rigid *fimbriae* are similar in external morphology to the spiked exine of pollen, and so Wenzel's law would increase the hydrophobicity and therefore the collection efficiency even further.

The difference in the collection efficiency between synthetic microparticles and pollen and *E. coli* suggests that the use of synthetic polymer microparticles as a model of device performance in the collection of biological materials[1] may be inappropriate; if possible, direct use of the biological microparticles in question would be more suitable for a particular evaluation. Since many microorganisms do not have smooth surfaces, in situations where the surface characteristics may be important, a variety of pollen species or at least *E. coli* bacteria may be more useful as a biological analog.

One must be careful to not take any particular value of the collection efficiency to assess the device's ability to collect particles. In this study, the method to collect particles was consistently the same, with the same device, input power, configuration, and operation protocol. The number of particles on the surface for all the tests was relatively high and homogeneous across the surface, and the collection speed was less than about a second. Further, for each test, the particles were homogeneous, rather than representing the situation that would be encountered in an actual application. However, the central focus of this work remains the mechanism by which the particles are collected. By changing the operation of the device, its configuration, and the nature of its application, the collection efficiency might be considerably different, and though these things are worthy of study, the understanding of the physics should come first. Ideally, the collection efficiencies would be closer to 100% if the device were intended for quantitative assessment of the particulates – an accurate count of the number of particles, for example – but the majority of applications for such a device are believed to be qualitative in nature, where lower collection efficiencies may be tolerated for the sake of simplicity and speed. The device may also be made far smaller by virtue of the nature of SAW devices generally, following the general trend of miniaturization of all sensors. However, the manipulation of droplets in the manner described in this work is possible from centimetre to micrometre scales, and in fact larger devices may enable the detection of far smaller amounts of target bioparticles with an ability to concentrate particulates from the droplet on the same device.[25]

Conclusions

Microparticle collection using a SAW device has been demonstrated in a form appropriate for use as a necessary step to the development of a useful miniaturized biosensor. The collection efficiency obtained for synthetic particles was found to be lower for larger hydrophobic polystyrene particles, and higher with larger hydrophilic melamine particles. The relationship between collection efficiency, particle size, and wettability is complex and is reliant on the ability of the recirculating fluid drop to overcome interfacial forces between the particles and the substrate to pick up and retain them until the droplet reaches the end of the track. The pressure distribution within the fluid is an important factor in particle collection using acoustic means to drive the droplet as well. The affinity of hydrophilic particles for water in the bulk of the droplet means that particle uptake into the bulk increases the more hydrophilic the particle or the greater its surface area. On the other hand, hydrophobic particles, especially the larger ones, tend to accumulate at the substrate towards the three-phase contact line about the periphery of the droplet to minimize its contact with water, thus explaining the formation of the monolayer ring-like assemblies.

The collection efficiency was far better with pollen, depending on the species; the efficiency for pollen was 45–68%, compared with 16–55% for synthetic particles. Curiously, the collection efficiency was relatively good for *E. coli* bacteria at *ca.* 61–70%, interesting given the hydrophobic and spiked surface of the bacteria, though consistent with our other results. The enhancement of the collection efficiency for pollen and the bacteria appeared to be at least partially due to the roughness of the pollen surface; Wenzel's law would appear to support this conclusion. Using pollen and *E. coli* instead of synthetic analogs in tests such as the one in this study should provide a better model in the collection of airborne microorganisms as these tiny bioparticles generally do not exist as smooth microspherical shapes. With this device, the collection of microorganisms *via* SAW indeed appears feasible.

Acknowledgements

The authors wish to acknowledge the assistance of Rick Barber at MiniFAB (Scoresby, Australia) in fabrication of the SAW devices, Professor Peter Kershaw (Centre for Palynology and Palaeocology, Monash University) for advice on suitable pollens and their characteristics, and Professor Ken-ya Hashimoto (Chiba Unversity, Japan) for detailed conversation on SAW devices.

References

1 Y. Zhao and S. K. Cho, 'Microparticle sampling by electrowetting-actuated droplet sweeping', *Lab Chip*, 2005, **6**, 137–144.
2 Z. Zhang, J. Zhe, S. Chandra and J. Hu, 'An electronic pollen detection method using Coulter counting principle', *Atmos. Environ.*, 2005, **39**, 5446–5453.
3 C. K. Campbell, *Surface Acoustic Wave Devices*, Academic, London, 1998.
4 S. Shiokawa and J. Kondoh, 'Surface acoustic wave sensors', *Jpn. J. Appl. Phys., Part 1*, 2004, **43**, 2799–2802.

5 A. Wixforth, 'Acoustically driven planar microfluidics', *Superlattices Microstruct.*, 2003, **33**, 389–396.
6 A. Wixforth, C. Strobl, Ch. Gauer, A. Toegl, J. Scriba and Z. von Guttenberg, 'Acoustic manipulation of small droplets', *Anal. Bionanal. Chem.*, 2004, **379**, 982–991.
7 C. J. Strobl, Z. von Guttenberg and A. Wixforth, 'Nano- and pico-dispensing of fluids on planar substrates using SAW', *IEEE Trans. Ultrason., Ferroelect., Freq. Control*, 2004, **51**, 1432–1436.
8 A. Renaudin, P. Tabourier, V. Zhang, J. C. Camart and C. Druon, 'SAW nanopump for handling droplets in view of biological applications', *Sens. Actuators, B*, 2006, **113**, 389–397.
9 M. Kurosawa, T. Watanabe, A. Futami and T. Higuchi, 'Surface acoustic wave atomizer', *Sens. Actuators, A*, 1995, **50**, 69–74.
10 M. Kurosawa, A. Futami and T. Higuchi, 'Characteristics of liquids atomization using surface acoustic wave', in *Solid-State Sensors and Actuators (Transducers), 1997 9th International Conference*, held in Chicago, IL, 16–19 June 1997, IEEE Press, New York, 1998, vol. 2, pp. 801–804.
11 K. Chono, N. Shimizu, Y. Matsui, J. Kondoh and S. Shiokawa, 'Novel atomization method based on SAW streaming', in *2003 IEEE Ultrasonics Symposium*, held 5–8 October 2003, Honolulu, Hawaii, IEEE Press, New York, 2004, vol. 2, pp. 1786–1789.
12 K. Chono, N. Shimizu, Y. Matsui, J. Kondoh and S. Shiokawa, 'Development of novel atomization system based on SAW streaming', *Jpn. J. Appl. Phys., Part 1*, 2004, **43**, 2987–2991.
13 J. J. Bang and L. E. Murr, 'Collecting and characterizing atmospheric nanoparticles', *JOM*, 2002, **54**(12), 28–30.
14 R. M. White and F. W. Voltmer, 'Direct piezoelectric coupling to surface elastic waves', *Appl. Phys. Lett.*, 1965, **7**, 314–316.
15 C. Glorieux, K. Van de Rostyne, K. Nelson, W. Gao, W. Lauriks and J. Thoen, 'On the character of acoustic waves at the interface between hard and soft solids and liquids', *J. Acoust. Soc. Am.*, 2001, **110**, 1299–1306.
16 T. Uchida, T. Suzuki and S. Shiokawa, 'Investigation of acoustic streaming excited by surface acoustic waves', in *1995 IEEE Ultrasonics Symposium*, held in Seattle, WA, 7–10 Nov 1995, IEEE Press, New York, 1995, vol. 2, pp. 1081–1084.
17 Sir J. Lighthill, 'Acoustic streaming', *J. Sound Vib.*, 1978, **61**, 391–418.
18 D. Hou and H. C. Chang, 'Electrokinetic particle aggregation patterns in microvortices due to particle–field interaction', *Phys. Fluids*, 2006, **18**, 071702.
19 D. J. Bakewell and H. Morgan, 'Quantifying dielectrophoretic collections of sub-micron particles on microelectrodes', *Meas. Sci. Technol.*, 2004, **15**, 254–266.
20 J. E. McDonald, 'Pollen wettability as a factor in washout by raindrops', *Science*, 1964, **143**, 1180–1181.
21 J. K. Varma, K. D. Greene, M. E. Reller, S. M. DeLong, J. J. Trottier, S. F. Nowicki, M. DiOrio, E. M. Koch, T. L. Bannerman, S. T. York, M. A. Lambert-Fair, J. G. Wells and P. S. Mead, 'An outbreak of *Escherichia coli* O157 infection following exposure to a contaminated building', *J. Am. Med. Assoc.*, 2003, **290**(20), 2709–2712.
22 M. A. Neill, P. I. Tarr, D. N. Taylor and A. F. Trofa, '*Escherichia coli*', in *Foodborne Disease Handbook*, ed. Y. H. Hui, J. R. Gorham, K. D. Murell and D. O. Cliver, Marcel Decker, Inc, New York, 1994, pp. 169–213.
23 Student, The probable error of a mean, *Biometrika*, 1908, **6**, 1–25.
24 M. Schindler, P. Talkner and P. Hänggi, 'Computing stationary free-surface shapes in microfluidics', *Phys. Fluids*, 2006, **18**, 103303.
25 H. Li, J. R. Friend and L. Y. Yeo, 'Surface acoustic wave concentration of particle and bioparticle suspensions', *Biomed. Microdev.*, 2006, accepted.
26 N. Aboobaker, D. Blackmore and J. Meegoda, 'Mathematical modeling of the movement of suspended particles subjected to acoustic and flow fields', *Appl. Math. Modell.*, 2005, **29**, 515–532.
27 D. Leighton and A. Acrivos, 'The shear-induced migration of particles in concentrated suspensions', *J. Fluid Mech.*, 1987, **181**, 415–439.
28 L. Y. Yeo, D. Hou, S. Maheshswari and H. C. Chang, 'Electrohydrodynamic surface microvortices for mixing and particle trapping', *Appl. Phys. Lett.*, 2006, **88**, 233512.
29 R. N. Wenzel, 'Resistance of solid surfaces to wetting by water', *Ind. Eng. Chem.*, 1936, **28**, 988–994.
30 J. De Coninck, J. Ruiz and S. Miracle-Solé, 'Generalized Young's equation for rough and heterogeneous substrates: A microscopic proof', *Phys. Rev. E*, 2002, **65**, 036139.
31 M. Rosenberg, D. Gutnick and E. Rosenberg, 'Adherence of bacteria to hydrocarbons: A simple method for measuring cell-surface hydrophobicity', *FEMS Microbiol. Lett.*, 1980, **9**, 29–33.